RSC Advances

PAPER

View Article Online
View Journal | View Issue

Cite this: *RSC Adv.*, 2020, **10**, 11418

Preparing and testing the reliability of long-afterglow $SrAl_2O_4:Eu^{2+}$, Dy^{3+} phosphor flexible films for temperature sensing

Li Wang,[a] Zhaojiang Shang,*[a] Mingming Shi,[a] Peiyuan Cao,[a] Bobo Yang[a] and Jun Zou *[ab]

Owing to its stability and environment-friendly properties, the $SrAl_2O_4:Eu^{2+}$, Dy^{3+} (SAOED) phosphor has attracted major scientific interest. With various applications, such as in emergency signage, luminous paints, and traffic signs, it can have a considerable impact on everyday activities. However, $SrAl_2O_4$ easily undergoes hydrolysis in the presence of atmospheric moisture. To remedy this, we prepared a phosphor film by spin coating to improve its water resistance. The SAOED was coated with epoxy resin glue without destroying the $SrAl_2O_4$ crystals. A series of reliability tests were conducted on the phosphor films and bare phosphors: high-temperature and high-humidity (HT) tests, thermal-cycling (TC) tests, and xenon lamp aging (XLG) tests. Then, the crystal phase, surface morphology, photoluminescence (PL), afterglow decay, and temperature-dependent PL were analyzed. The X-ray diffraction patterns show that the hydrolysis reaction of SAOED occurred easily, with the $SrAl_2O_4$ phase becoming the $Sr_3Al_2(OH)_{12}$ phase and $SrAl_3O_5(OH)$ generated under HT tests. The PL intensity of the thin film of SAOED decreased 57.2%, 79.3%, and 98.8% after HT tests, XLG tests for 168 h, and TC tests with 10 repetitions from 233 K to 423 K, respectively. Moreover, the afterglow decay time of the SAOED phosphor film was longer than that of bare phosphors. The developed flexible films are excellent candidates for temperature sensing because they exhibit temperature-dependent PL intensity and are highly sensitive to surrounding temperature variation 300–420 K. Thus, SAOED films with stable luminescent signals can be used in energy-efficient, long-lasting temperature-sensing devices, which, apart from being environment-friendly, play a role in improving public safety infrastructure.

Received 20th January 2020
Accepted 4th March 2020

DOI: 10.1039/d0ra00628a

rsc.li/rsc-advances

1. Introduction

Long-persistent phosphors exhibit an energy-saving luminescence process whereby energy can be absorbed *via* traps under sunlight, or ultraviolet (UV) illumination.[1,2] Europium and dysprosium co-doped $SrAl_2O_4$ is a highly efficient green-emitting phosphor; its afterglow time can be observed up to 30 h after the termination of excitation. Europium ion-doped alkaline-earth aluminate compounds are promising phosphors featuring broad emission in the UV-visible range owing to the 5d–4f transitions of Eu^{2+}.[3] Specifically, $SrAl_2O_4$ insulators have a wide bandgap and are doped with rare earth elements such as Dy or Nd, which form structural defects to help increase the recombination time of the electron–hole pair.[4,5]

Recently, the $SrAl_2O_4:Eu^{2+}$, Dy^{3+} phosphor has received considerable research attention because of its stability and environmentally friendly properties, with various applications such as emergency signage, watch dials, luminous paints, traffic signs, and children's toys.[6–10] There are many techniques to manufacture strontium aluminate, such as sol–gel synthesis,[7] continuous solid-phase synthesis,[11] combustion,[12] and high-temperature solid-state method.[13] The high-temperature solid-state method synthesizes the phosphor with the highest crystallinity. Push laser deposition and the sol–gel method are new and developing technologies that can improve the phosphor luminous reliability of flexible phosphor film.[14–17] However, $SrAl_2O_4$ easily undergoes hydrolysis in water environments with little hindrance. In order to improve SAOED reliability, the surface coating and decoration is a new research field.[18,19] The epoxy resin coating phosphors film can improve phosphor water resistance and compatibility with affiliated luminescent signals.[20]

Epoxy resins are important optical material, which have high chemical resistance, excellent weather resistance, low cost-effectiveness and low toxicity, and excellent transparency.[21,22] This paper uses the long afterglow SAOED phosphors, which has high luminous efficiency and good chemical stability, and epoxy resin to make up the flexible phosphor film with good optical property and reliability. In addition, SAO:Eu^{2+}, Dy^{3+} film

[a]*School of Science, Shanghai Institute of Technology, Shanghai 201418, PR China. E-mail: zoujun@sit.edu.cn; shangzj@sit.edu.cn*

[b]*Institute of New Materials & Industrial Technology, Wenzhou University, Wenzhou 325024, PR China*

can be used for temperature sensing, in energy-efficient and long-lasting automotive and public safety infrastructure.[23,24]

Currently, there is an urgent demand for the development of superior flexible film devices based on long afterglow phosphors that exhibit stable luminescent signals. Specifically, the development of temperature-sensitive luminescent materials is particularly important for the fabrication of temperature sensors. In this study, a film consisting of SAOED, and epoxy resin is created by spin-coating. To verify the reliability of the developed film, high-temperature and high-humidity (HT) tests are employed as an accelerated lifetime test (to determine water resistance of the film),[25] as well as thermal cycling (TC) tests and xenon lamp aging (XLG) tests. The afterglow decay time of long afterglow phosphors, which have been the subject of extensive research focusing specifically on the mechanism behind producing optical phenomenon are further extended.[26] Finally, the afterglow decay time, crystal structure and morphology, the photoluminescence (PL) properties, and temperature-dependent PL are analyzed and discussed.

2. Experimental

2.1 Preparation of phosphor films

In this study, flexible SAOED phosphors films were prepared by the spin coating method (Fig. 1). Green $SrAl_2O_4:Eu^{2+}$, Dy^{3+} phosphors (JPA-388, Guangzhou, Juliang), Glue A (5351A, Shanghai Huitian), and Glue B (5351B, Shanghai Huitian) were used as the raw materials. The phosphors and epoxy resin were thoroughly mixed (to a Glue A : Glue B : SAOED phosphors ratio of 5 : 5 : 1) and stirred constantly. Then, the mixture was placed into a vacuum deaerator and removed after 5 min to reduce the number of bubbles in the luminescent film. The film was then formed using a coating method with a glue-leveling mechanism. After the layers were finished, the phosphor films were placed in an oven at 80 °C for 30 min and 150 °C for 30 min.

2.2 Reliability tests and measurements

The bare phosphors and phosphor films were tested for reliability exposure using xenon lamps for 168 h (XLG tests); high temperature and humidity (T: 85 °C, RH: 85%) for 168 h (HT tests) and 10 repetitions of thermal-cycling from 233 to 393 K (TC tests). The crystallized phase structures of strontium aluminate samples before and after the three reliability

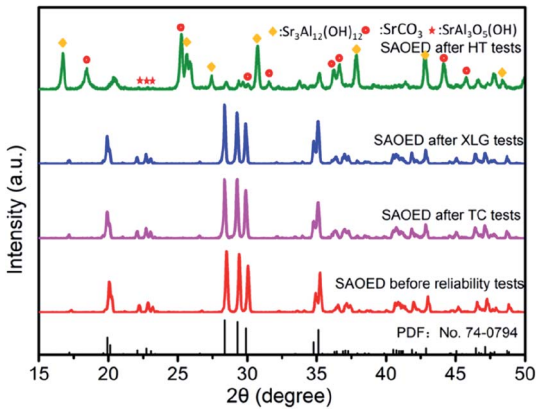

Fig. 2 XRD patterns of $SrAl_2O_4:Eu^{2+}$, Dy^{3+} phosphors and samples after high-temperature and high-humidity (HT) tests; xenon lamp aging (XLG) tests; and thermal-cycling (TC) tests.

experiments, as well as strontium aluminate samples without the aging experiment, were confirmed by X-ray diffraction (XRD) (Rigaku, Ultima IV, Japan) with Cu Kα radiation (k = 0.154178 nm) operating at 40 kV and 40 mA, over a 2θ range from 10–80°at a scanning rate of 0.02° per step and 2° min^{-1}. PL and PL excitation (PLE) spectra were recorded using an Edinburgh Instruments (Edinburgh, UK) FS5 spectrofluorometer, using a xenon lamp as a light source. The morphological structure of the phosphors was observed with a Phenom Pro scanning electron microscope (SEM), whereas the films were examined by spectrofluorometric analysis and spectrophotometry to acquire of temperature-dependent PL data. A FJ427-A1 thermally stimulated spectrometer (Nuclear Industry, China) was used to investigate the afterglow decay phenomenon and analyze the trap energy level.

3. Results and discussion

3.1 Phase identification and morphology

Fig. 2 shows the XRD patterns of SAOED phosphors, which reveal that the host lattice is $SrAl_2O_4$ (PDF no. 74-0794), with the $P2_1(4)$ space group. The TC and XLG tests led to minimal destruction of the crystal structure, and the small band widths and absence of a broad background in the diffractogram indicate that the phosphors retained their high crystallinity.

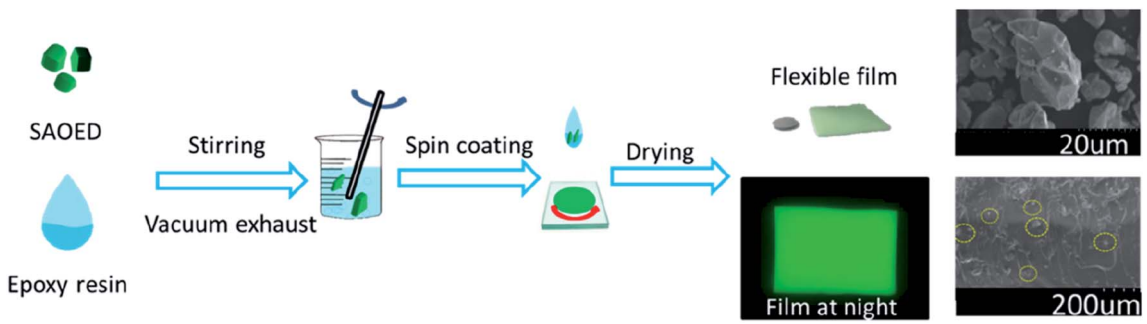

Fig. 1 Schematic showing the preparation of flexible SAOED phosphor films for temperature sensing.

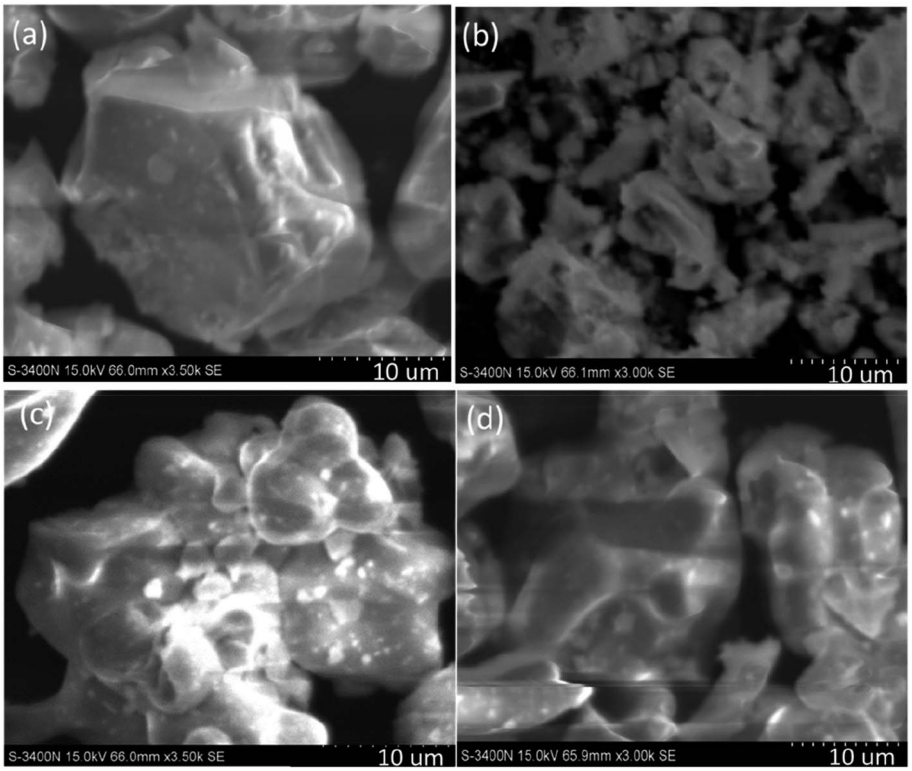

Fig. 3 SEM images showing the morphologies of four types of phosphors: (a) before reliability tests; (b) after high-temperature and high-humidity (HT) tests; (c) after thermal cycling (TC) tests, and (d) after xenon lamp aging (XLG) tests.

However, a clear change was observed after the HT aging tests, whereby the SAOED is hydrolyzed to new substances and the principal crystalline phase of the phosphor transforms to $Sr_3Al_2(OH)_{12}$ (PDF no. 24-1186),[27–29] mixed with impurity-phases: $SrCO_3$, $SrAl_3O_5(OH)$, and some $SrAl_2O_4$. The hydrolysis process can be expressed as follows:

$$7SrAl_2O_4 + 8H_2O \rightarrow Sr_3Al_2(OH)_{12} + 4SrAl_3O_5(OH) \quad (1)$$

$$SrAl_2O_4 + 4H_2O \rightarrow Sr^{2+} + 2OH^- + Al(OH)_3 \quad (2)$$

$$Sr^{2+} + 2OH^- + CO_2 \rightarrow SrCO_3 + H_2O \quad (3)$$

This indicates that the SAOED is not stable in a high humidity environment; instead, it will decompose into a mixture of $Sr_3Al_2(OH)_{12}$ and $SrAl_3O_5(OH)$, and strontium ions will react with carbon dioxide in the air to form strontium carbonate.

Fig. 3 shows a SEM image of the $SrAl_2O_4:Eu^{2+}$, Dy^{3+} phosphor before and after the three reliability tests. The phosphors in Fig. 3a exhibit well-developed crystal faces, resulting in a smooth surface and relatively little particle aggregation, with some sharp projections on the crystal surface. SEM images of SAOED phosphors after exposure to high temperature (85 °C) and high humidity (85%) reveal substantial changes in the phosphors (Fig. 3b), characterized by deep erosion of the crystal

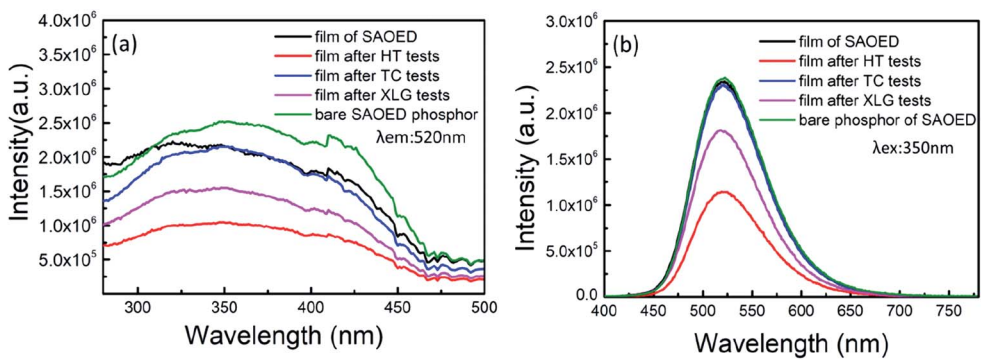

Fig. 4 (a) PL excitation spectra and (b) PL spectra of the SAOED phosphors and film before and after the three aging tests.

surface and transformation of the phosphors into $Sr_3Al_2(OH)_{12}$, $SrCO_3$, and $SrAl_3O_5(OH)$.[27–29] Moreover, the surface of the phosphors exhibits substantial flocculent precipitate after the HT tests. After TC and XLG tests, the phosphor grains start to aggregate, resulting in a larger crystal size, which reduces the luminous intensity of the SAOED phosphors (Fig. 3c and d).

3.2 Photoluminescence properties

Fig. 4a shows the PLE spectra of SAOED films before and after the three reliability tests, as well as the PLE spectra of bare SAOED. The observed excitation of all samples is similar to that reported in the literature;[30] the maximum wavelength of excitations is approximately 350 nm and a straightforward $4f^65d^1 \rightarrow 4f^7$ transition of the Eu^{2+} ion is observed.[31] Fig. 4b shows the PL emission spectra of the SAOED phosphors and SAOED film before the reliability tests, as well as those of the phosphor films after the three reliability tests. The luminescence peaks of the phosphors and films are all located near the 520 nm emission peak, which represents the typical location of $4f^65d^1 \rightarrow 4f^7$ where the transition emission peak of Eu^{2+} and the emission center of Eu are in two different Sr crystal positions.[32–34] The

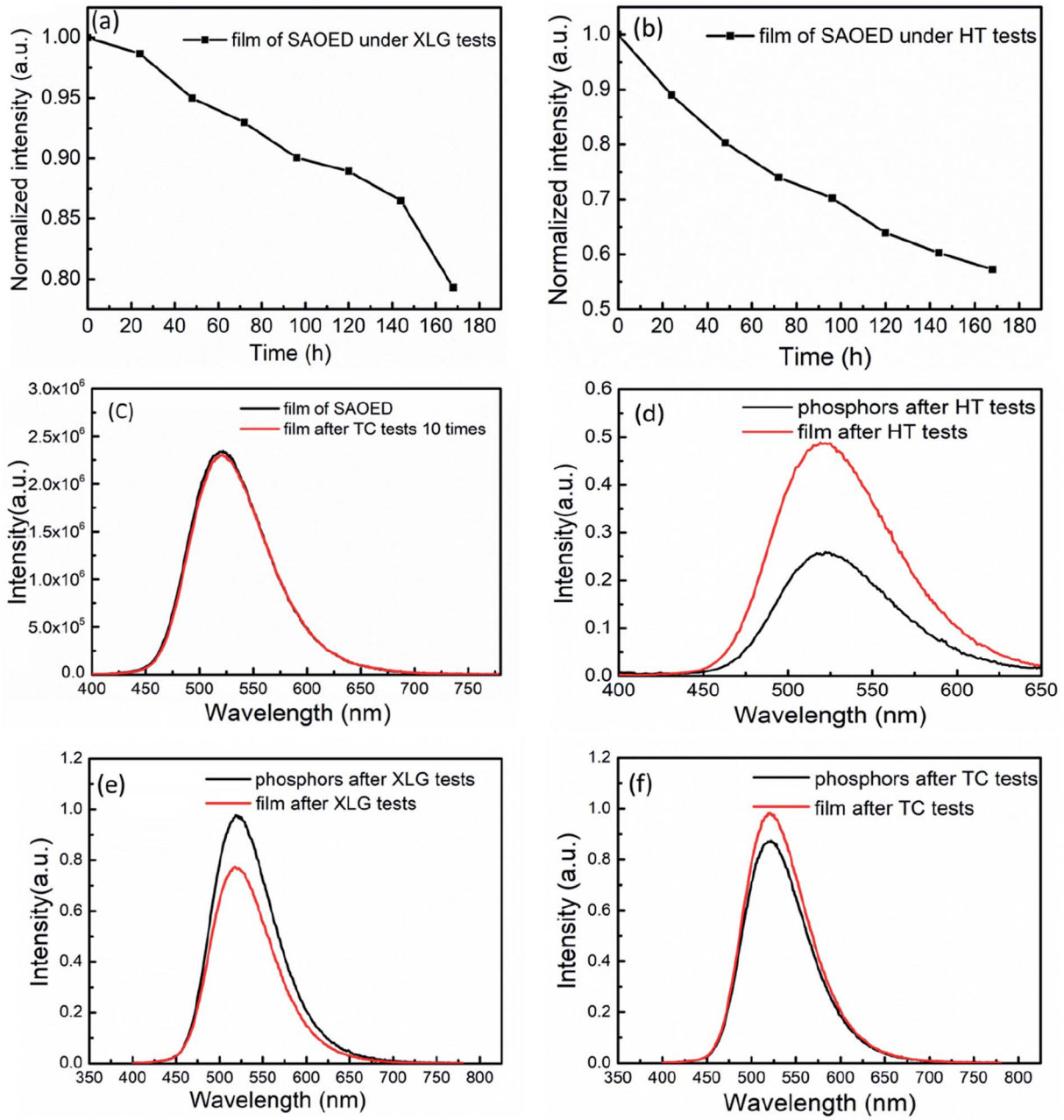

Fig. 5 (a) PL emission spectra of the phosphor film under ambient conditions of 85 °C/85% RH with aging time (HT tests); (b) under xenon lamp aging with aging time (XLG tests); (c) and before and after TC tests; (d–f) PL emission spectra of the phosphors and films after the three reliability tests.

epoxy resin is an excellent coating material compared to SiO_2 and BN,[18,19] because the PL peaks of bare phosphors and phosphors film are basically coincide.

The reliability tests do not result in changes to the strongest emission wavelength; the shapes of the PL emission and excitation spectra of the SAOED phosphor film and SAOED phosphor are approximately equal. The HT tests have the greatest influence on the PL intensity of these samples, followed by XLG tests, and then TC tests. The peak PL intensity exhibits a rapid decline of 54.1% under the high-temperature and high-humidity environment for 168 h. This is because water molecules meet the strontium aluminate *via* the hydrogen bonds of epoxy resin and the film gap, resulting in hydrolysis of the strontium aluminate in the film.[35] The emission peak only declines by 1.2% after the TC tests, which indicates excellent repeatability of the film as a temperature measuring device.

3.3 Reliability tests

The luminescence intensity of the SAOED film decreases by 19.7% after xenon aging and 48.7% after HT tests, whereas it increases by 1.2% after TC tests (Fig. 5a–c). Fig. 5d–f shows the PL emission spectra of the SAOED phosphors and film after the reliability tests. The thin phosphor film is more stable than SAOED phosphors in the high-temperature and high-humidity environment because the phosphors cannot directly react with water; instead, the water molecules slowly permeate the phosphor film. However, the phosphors exhibit higher PL emission intensity than the film after XLG tests. This may be because the film was kept at 65 °C for 168 h, which might be too high a temperature to induce changes in the film. Additionally, the phosphor film exhibits greater thermal stability than the SAOED phosphor after the TC tests. In summary, compared with other coating methods,[18,19] epoxy resin coating phosphor film has two advantages. One is that it hardly impact on the optical performance of SAOED. The other is that the water resistance of SAOED increases by 99.8%.

3.4 Afterglow behavior

The afterglow decay characteristics of the SAOED phosphors and phosphor films are shown in Fig. 6a and b, respectively. This decay can be expressed by the following equation:

$$\frac{dn_t}{dt} = \frac{-\alpha n_t^2}{n_t + (b/r) \times (N - n_t)} \quad (4)$$

where N is the trap concentration, n_t is the number of electrons in the trap states, α is the probability that a trapped electron is thermally excited into the conduction band, b is the probability that the leased free electron is captured by another trap, and r the probability that the electron recombines with a hole.

In this study, the afterglow of the prepared SAOED phosphors is very light; it is maintained for a few hours in daylight. This afterglow behavior indicates that the trap saves high energy particles. The function of the after decay can be calculated by the following equation:

$$f = y_0 + A_1 e^{(-t/\tau_1)} + A_2 e^{(-t/\tau_2)} \quad (5)$$

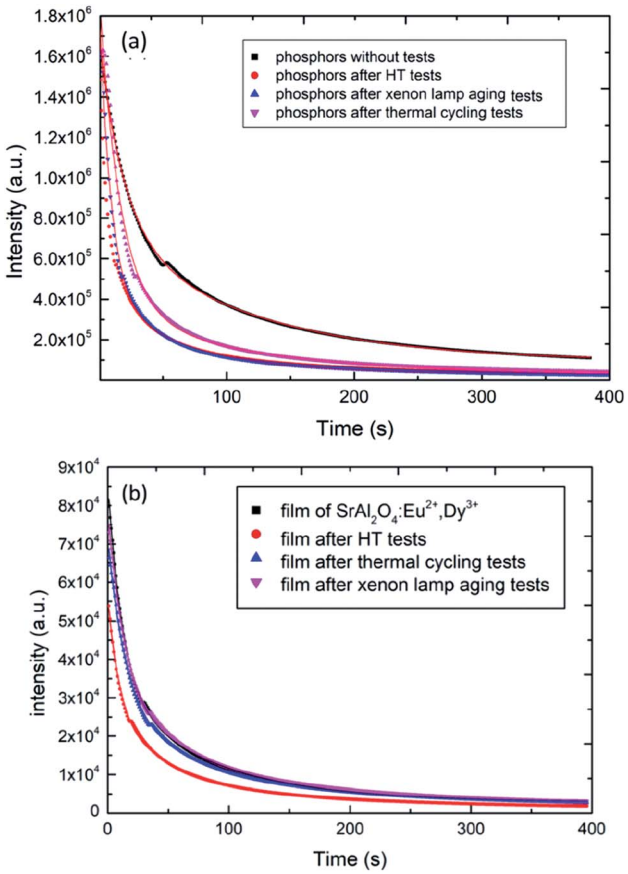

Fig. 6 (a) Afterglow decay curves of the SAOED phosphors and the sample after reliability tests, (b) afterglow decay curves of the films and the sample after reliability tests.

where f is the phosphorescent intensity, τ_1 and τ_2 are the afterglow decay times, A_1 and A_2 are constants, and t is the time. The afterglow decay time of the phosphor reflects t the level of the trap energy band after the reliability tests. The film process protects the phosphor from drastic environmental changes. The afterglow decay times, τ_1 and τ_2, for the phosphors and films correspond to a two-decay process: fast decay and slow decay. The τ_1 value of the film is approximately 20 s, which is longer than that of the phosphor, indicating a fast afterglow decay process where particles caught in the trap jump from a high energy state to a low energy state by thermal motion. The τ_2 value is the longer decay time and indicates a deeper level of the trap, corresponding to a slow afterglow decay process. Furthermore, according to the reliability test results, the decay times are longer for the films than the phosphors; thus, the phosphor films are more stable than the bare phosphors (Fig. 7).

3.5 Temperature-dependent PL characteristics

The radiation-free transition rate is temperature dependent. In many luminescent materials, the increase of temperature reduces the luminous efficiency and leads to temperature quenching, caused by the non-radiative transition of the

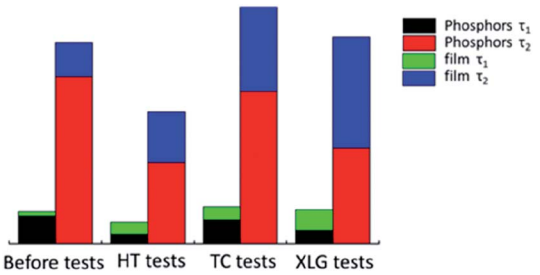

Fig. 7 Decay times (τ_1 and τ_2) of phosphor and phosphor film before and after the reliability tests.

downward energy level. PL intensity of the phosphors decreases with increasing temperature due to an increased probability of non-radiative transitions.[36–39] The temperature-depended PL intensity may be fitted with the Arrhenius equation:

$$I(T) = \frac{I(0)}{1 + \frac{\Gamma_0}{\Gamma_v}\exp(-\Delta E/k_b T)} \quad (6)$$

where I_0 and $I(T)$ are the intensity at temperature $T = 0$ and T (K), respectively; k_b is the Boltzmann constant; Γ_v is the radiative decay rate of the 5d state; Γ_0 is the attempt rate for thermal quenching; ΔE is the energy barrier for the thermal quenching process. Thermal expansion of the host lattice and enhanced interactions between the 5d electrons and phonons at elevated temperatures also result in thermal shifts of the emission maxima of Eu^{2+} activated phosphors. Fig. 8a shows the temperature dependent PL spectra of SAOED phosphors excited at 350 nm. The PL intensity decreases with increasing temperature. Then, as the temperature drops from 420 to 300 K, the intensity increases back to 95% of the original. Fig. 8b and c show the reduction in emission intensity of the phosphor films with increasing temperature from 300 to 420 K and 300 to 360 K, respectively. Fig. 8d reveals that the emission intensity of the film exhibits excellent linearity with increasing temperature from 300–360 K. The PL emissions revealed that the phosphor films were highly sensitive to surrounding temperature variations (300–420 K) and had a strong linear behavior despite their sensitivity. These flexible and soft phosphor films with a strong temperature response, strong light-induced scattering, and good flexibility are excellent prospective candidates for temperature sensor devices in harsh industrial environments.

4. Summary

This study determined the phase identification, morphology, photoluminescence, and afterglow decay time of SAOED film and phosphors after three types of reliability tests. The results revealed that the reliability of the film increased after the tests. HT tests had the greatest influence on the phosphors, followed by TC tests, then XLG tests. HT tests also had the greatest influence on the phosphor films; after HT tests, the reliability of the film increased to 187.5%. The XRD results show that the phosphor was more prone to hydrolysis than the film.

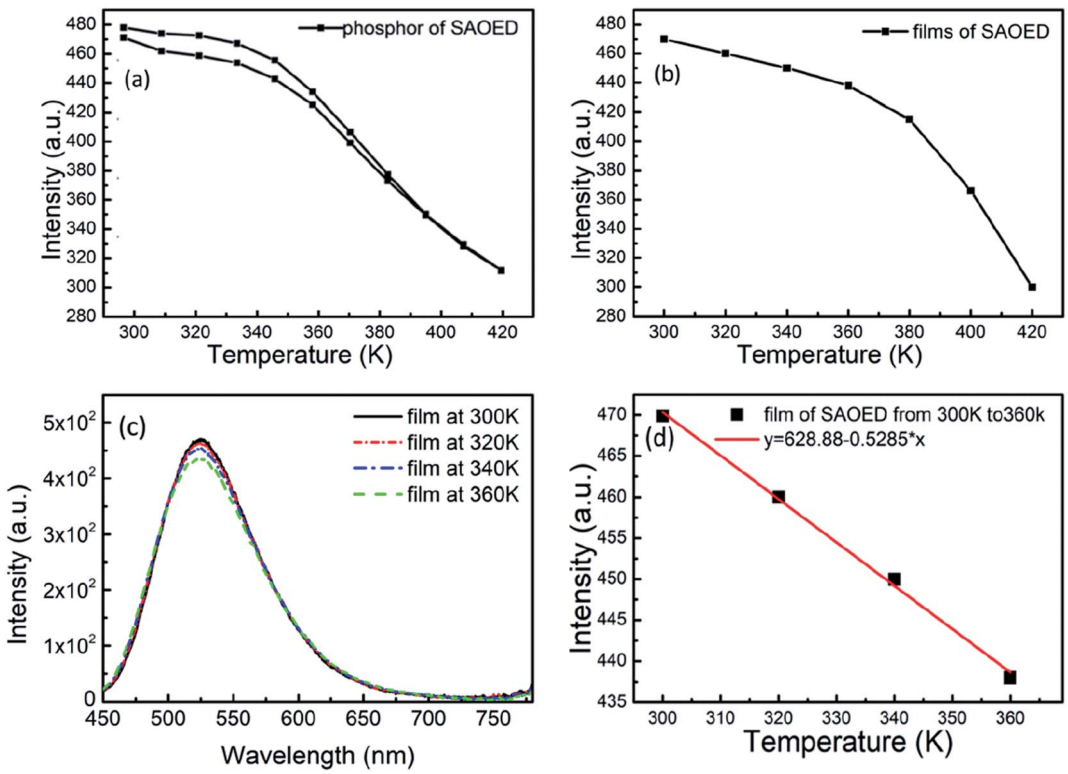

Fig. 8 Temperature-dependent PL emission spectra of (a) SAOED phosphors and (b) SAOED phosphor films. (c) PL emission intensity of SAOED phosphor films at 300–360 K. (d) Temperature-dependent intensity of SAOED phosphor films at 300–360 K.

Moreover, the afterglow decay time revealed the situation which led to defects in SAOED. Furthermore, temperature-dependent PL showed that the phosphor film and SAOED phosphors are thermally stable. However, although the phosphor film improved the SAOED reliability, the reason for the good linearity of the SAOED film PL intensity was not found at 300–360 K, and the afterglow mechanism of the film after a long duration was not verified. The film water permeability experiment did not further verify the hydrolysis of SAOED film. In summary, the overall results show that phosphor film is more reliable than bare phosphor because the epoxy resins coat the phosphor and increase its water resistance. These results can help increase the application of SAOED in public safety infrastructure among other industries.

Conflicts of interest

There are no conflicts to declare.

Acknowledgements

This work was supported by the National Natural Science Foundation of China (61901270), the Shanghai Sailing Program (17YF1419200) and the Science and Technology Planning Project of Zhejiang Province, China (2018C01046).

References

1 E. Finley, A. Mansouri Tehrani and J. Brgoch, Intrinsic Defects Drive Persistent Luminescence in Monoclinic $SrAl_2O_4$:Eu^{2+}, *J. Phys. Chem. C*, 2018, **122**(28), 16309–16314.

2 A. S. Paterson, B. Raja, V. Mandadi, *et al.*, A low-cost smartphone-based platform for highly sensitive point-of-care testing with persistent luminescent phosphors, *Lab Chip*, 2017, **17**(6), 1051–1059.

3 D. Ravichandran, S. T. Johnson, S. Erdei, *et al.*, Crystal chemistry and luminescence of the Eu^{2+}-activated alkaline earth aluminate phosphors, *Displays*, 1999, **19**(4), 197–203.

4 T. Maldiney, C. Richard, J. Seguin, *et al.*, Effect of core diameter, surface coating, and PEG chain length on the bio distribution of persistent luminescence nanoparticles in mice, *ACS Nano*, 2011, **5**(2), 854–862.

5 A. S. Paterson, B. Raja, G. Garvey, *et al.*, Persistent luminescence strontium aluminate nanoparticles as reporters in lateral flow assays, *Anal. Chem.*, 2014, **86**(19), 9481–9488.

6 W. M. Yen, S. Shionoya and H. Yamamoto, *Handbook, Phosphor.*, 2007.

7 V. D. E. Koen, P. F. Smet and D. Poelman, Persistent Luminescence in Eu^{2+}-Doped Compounds: A Review, *Materials*, 2010, **3**(4), 2536–2566.

8 N. M. Son, L. T. T. Vien, L. V. K. Bao and N. N. Trac, Synthesis of $SrAl_2O_4$:Eu^{2+}, Dy^{3+}phosphorescence nanosized powder by combustion method and its optical properties, *J. Phys.: Conf. Ser.*, 2009, **187**, 1–6.

9 N. M. Son, L. T. T. Vien, L. V. K. Bao and N. N. Trac, Synthesis of $SrAl_2O_4$:Eu, Dy phosphor nanometer powders by sol–gel processes and its optical properties, *Mater. Chem. Phys.*, 2004, **85**, 68–72.

10 V. Liepina, D. Millers, K. Smits, A. Zolotarjovs and I. Bite, X-ray excited luminescence of $SrAl_2O_4$:Eu, Dy at low temperatures, *J. Phys. Chem. Solids*, 2014, **115**(2018), 381–385.

11 B. Kerbel, *et al.*, Use of continuous solid-phase synthesis to obtain phosphors based on strontium aluminate, *Buech. Augenarztes*, 2016, **73**(1), 24.

12 R. Sharma, D. P. Bisen and B. P. Chandra, Mechanoluminescence of Dy doped strontium aluminate nanophosphors, *J. Lumin.*, 2015, **168**, 49–53.

13 X. Wei, Q. Jun, W. Haoyi, *et al.*, Structure and luminescence properties of $SrAl_2O_4$:Eu^{2+}, Dy^{3+} by Ba^{2+} and Ca^{2+} co-doping, *J. Alloys Compd.*, 2012, **514**, 97–102.

14 S. T. S. Dlamini, H. C. Swart and O. M. Ntwaeaborwa, Photoluminescence properties of $Y_3(Al,Ga)_5O_{12}$:Ce^{3+} thin phosphor films grown by pulsed laser deposition, *Phys. B*, 2014, **439**, 88–92.

15 I. B. Huang, *et al.*, Preparation and luminescence of green-emitting $ZnAl_2O_4$:Mn^{2+} phosphor thin films, *Thin Solid Films*, 2014, **570**, 451–456.

16 T. Kyômen, M. Hanaya and H. Takashima, Electroluminescence near interfaces between (Ca,Sr) TiO_3:Pr phosphor and SnO_2:Sb transparent conductor thin films prepared by sol–gel and spin-coating methods, *J. Lumin.*, 2014, **149**, 133–137.

17 A. Klausch, *et al.*, Wet chemical preparation of YVO_4:Eu thin films as red-emitting phosphor layers for fully transparent flat dielectric discharge lamp, *Thin Solid Films*, 2012, **520**(13), 4297–4301.

18 M. A. Sikandar, W. Ahmad, M. H. Khan, F. Ali and M. Waseem, Effect of water resistant SiO_2 coated $SrAl_2O_4$:Eu^{2+} Dy^{3+} persistent luminescence phosphor on the properties of Portland cement pastes, *Constr. Build. Mater.*, 2019, **228**, 116823.

19 J. Lin, Y. Huang, J. Zhang, F. Shi, S. Wei, J. Gao and C. Tang, Fabrication of BN nanosheets-coated $SrAl_2O_4$:Eu^{2+} as a new water-resistant phosphor by a one-pot method, *Mater. Chem. Phys.*, 2008, **108**(2–3), 440–444.

20 Y. Liu, J. Zou, B. Yang, *et al.*, Preparation and reliability of flexible phosphor film for warm white LED, *Mater. Technol.*, 2017, 1–7.

21 M. A. El-Rahman, K. M. Yassien and A. A. M. Yassene, Effect of gamma irradiation on the optical properties of epoxy resin thin films, *Optik*, 2019, **183**, 962–970.

22 H. V. Ramakrishna and S. K. Rai, Effect on the mechanical properties and water absorption of granite powder composites on toughening epoxy with unsaturated polyester and unsaturated polyester with epoxy resin, *J. Reinf. Plast. Compos.*, 2006, **25**(1), 17–32.

23 L. Zhang, S. Lyu, Q. Zhang, Y. Wu, C. Melcher, S. C. Chmely, Z. Chen and S. Wang, Dual-emitting film with cellulose nanocrystal-assisted carbon dots grafted $SrAl_2O_4$, Eu^{2+}, Dy^{3+} phosphors for temperature sensing, *Carbohydr. Polym.*, 2019, **206**, 767–777.

24 S. H. Tatumi, A. d. F. Soares, D. R. G. Tudela, K. A. Gonçalves and R. R. Rocca, Sol-gel synthesis of strontium aluminate phosphor and its TL and OSL properties, *Radiat. Phys. Chem.*, 2019, **157**, 15–21.

25 I. Bite, G. Krieke, A. Zolotarjovs, *et al.*, Novel method of phosphorescent strontium aluminate coating preparation on aluminum, *Mater. Des.*, 2018, **15**, 794–802.

26 Y. Liu, *et al.*, Effect of gallium ion content on thermal stability and reliability of YAG: Ce phosphor films for white LEDs, *Ceram. Int.*, 2018, **44**(1), 1091–1098.

27 E. Finley, A. Mansouri Tehrani and J. Brgoch, Intrinsic Defects Drive Persistent Luminescence in Monoclinic $SrAl_2O_4$: Eu^{2+}, *J. Phys. Chem. C*, 2018, **122**(28), 16309–16314.

28 P. Ptáek, *et al.*, Synthesis, hydration and thermal stability of hydrates in strontium-aluminate cement, *Ceram. Int.*, 2014, **40**(7), 9971–9979.

29 K. V. Zakharchuk, A. A. Yaremchenko and D. P. Fagg, Electrical properties and thermal expansion of strontium aluminates, *J. Alloys Compd.*, 2014, **613**, 232–237.

30 H. Lv, Z. Pan and Y. Wang, Synthesis and mechanoluminescent property of (Eu^{2+},Dy^{3+})-co-doped strontium aluminate phosphor by soft mechanochemistry-assisted solid-state, *J. Lumin.*, 2019, **209**, 129–140.

31 W. Jia, H. Yuan, S. Holmstrom, H. Liu and W. M. Yen, Photo-stimulated luminescence in $SrAl_2O_4$: Eu^{2+}, Dy^{3+} single crystal fibers, *J. Lumin.*, 1999, **83–84**(99), 465–469.

32 J. R. Qiu, K. Miura, H. Inouye, *et al.*, Blue emission induced in Eu^{2+}-doped glasses by an infrared femtosecond laser, *J. Non-Cryst. Solids*, 1999, **244**(1), 185–188.

33 Y. M. Huang and Q. L. Ma, Long afterglow of trivalent dysprosium doped strontium aluminate, *J. Lumin.*, 2015, **160**, 271–275.

34 S. Park, S. Park, D. H. Jang, H. S. Lee and C. H. Park, Anti-fogging behavior of water-absorbing polymer films derived from isosorbide-based epoxy resin, *Mater. Lett.*, 2016, **180**, 81–84.

35 C. Guo, L. Luan, D. Huang, *et al.*, Study on the stability of phosphor $SrAl_2O_4$:Eu^{2+}, Dy^{3+} in water and method to improve its moisture resistance, *Mater. Chem. Phys.*, 2007, **106**(2–3), 268–272.

36 S. Yan, On the origin of temperature dependence of the emission maxima of Eu^{2+} and Ce^{3+} - activated phosphors, *Opt. Mater.*, 2018, **79**, 172–185.

37 Y. Wu, H. Shi, B. C. Chakoumakos, M. Zhuravleva, M. H. Du and C. L. Melcher, Crystal structure, electronic structure, temperature-dependent optical and scintillation properties of $CsCe_2Br_7$, *J. Mater. Chem. C*, 2015, **3**(43), 11366–11376.

38 L. Zhang, S. Lyu, Q. Zhang, Y. Wu, C. Melcher, S. C. Chmely and S. Wang, Dual-emitting film with cellulose nanocrystal-assisted carbon dots grafted $SrAl_2O_4$, Eu^{2+}, Dy^{3+} phosphors for temperature sensing, *Carbohydr. Polym.*, 2019, **206**, 767–777.

39 J. C. G. Bünzli and K. L. Wong, Lanthanide mechanoluminescence, *J. Rare Earths*, 2018, **36**(1), 1–41.